



Cite this: *RSC Adv.*, 2017, 7, 37596

# Notable *in situ* surface transformation of Cu<sub>2</sub>O nanomaterials leads to dramatic activity enhancement for CO oxidation

Dan Zhao, \* Chang-Man Tu, Xue-Jing Hu and Ning Zhang\*

Cu<sub>2</sub>O is an important compound for many promising applications; however, its real state under serious application conditions, such as redox atmosphere of catalysis reactions, has seldom been investigated. In this study, a dramatic and sustainable activity enhancement for CO oxidation on catalytically used Cu<sub>2</sub>O nanoporous sphere samples was discovered as compared to that on their fresh counterparts. To illustrate the phenomenon, comprehensive characterizations such as XRD, H<sub>2</sub>-TPR, TEM, XPS, and CO-TPD were performed on fresh and used Cu<sub>2</sub>O samples. It was found that after one or several catalytic runs, the main phase among the used samples retained the crystalline feature of Cu<sub>2</sub>O. However, the surface would transform into a stable multivalent composite interface with almost unchanged Cu(II) : Cu(I) ratio (around 4.0) and active oxygen distribution, even after only one catalytic run for CO oxidation; this indicated a notable reaction-induced or *in situ* surface restructuring effect of the Cu<sub>2</sub>O substrates. Compared to that of pure Cu<sub>2</sub>O, CuO, and reported Cu<sub>x</sub>O samples, the active chemisorbed oxygen on these *in situ* restructured samples was observed in particularly higher surface composition (with the ratio of chemisorbed oxygen to lattice oxygen being around 5.5); this was further demonstrated to be highly efficient for the oxidization of CO in a relatively low temperature range even in the absence of O<sub>2</sub> in the atmosphere and could be the main contributor to speed up CO oxidation in these samples. A similar enhancement in the activity on the used samples for CO oxidation as compared to that on the fresh samples was further testified in Cu<sub>2</sub>O nanomaterials with different morphologies such as cubic, octahedral, and 18-facet polyhedral nanoparticles; this implied that the surface restructuring effect under a redox reaction atmosphere was a common feature of the Cu<sub>2</sub>O-based materials, and the transformed surface could act as a superior and stable interface for heterogeneous catalysis. These findings might help in recognizing the real state of Cu<sub>2</sub>O-containing materials under serious application conditions or designing highly efficient Cu<sub>2</sub>O-based materials *via* convenient atmosphere-controlled manipulation for advanced applications.

Received 27th May 2017

Accepted 17th July 2017

DOI: 10.1039/c7ra05950g

rsc.li/rsc-advances

## 1. Introduction

As one of the earliest used metals in human history, copper is basically featured by its stable existent forms, such as Cu, Cu<sub>2</sub>O, and CuO, with multiple oxidation states under ambient conditions, which offers wide applications ranging from roofing and plumbing material to electrical transmission and power generation. Among the popular Cu compounds, cuprous oxide (Cu<sub>2</sub>O) is extraordinarily attractive due to its non-stoichiometric p-type semiconductor property<sup>1,2</sup> and its prospective applications in gas sensing,<sup>3,4</sup> CO oxidation,<sup>5,6</sup> photocatalysis,<sup>7,8</sup> photocurrent generation,<sup>9,10</sup> and organic synthesis.<sup>11,12</sup> It is believed that the physical or chemical properties involved in the surface or interface structure of Cu<sub>2</sub>O-based materials directly

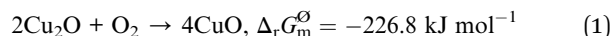
govern their performance. For instance, it had been reported that when Cu<sub>2</sub>O nanoparticles in different shapes were employed, the crystalline Cu<sub>2</sub>O surface plays an important role in CO oxidation<sup>13,14</sup> and photocatalytic decomposition of dyes.<sup>15,16</sup> In addition, the strategy of combining Cu<sub>2</sub>O on ZnO or TiO<sub>2</sub> substrates to form a composite interface was also functional to enhance the efficiency of the solar cells<sup>17</sup> or the photocatalytic activity for CO<sub>2</sub> reduction to methanol.<sup>18</sup> These studies focused on deliberate surface manipulations made the main contribution to the current innovation of Cu<sub>2</sub>O-based materials.<sup>19</sup>

However, it should be noted that the possible deviation of Cu<sub>2</sub>O from its metastable property and the corresponding influences have seldom been considered; this can lead to misinterpretation of functions of its real state for practical processes, especially under some special application conditions. For instance, Cu<sub>2</sub>O has been directly employed or composited with other components for some important

Institute of Applied Chemistry, College of Chemistry, Nanchang University, Nanchang, Jiangxi, 330031, China. E-mail: zhaodan@ncu.edu.cn; nzhang.ncu@163.com; Tel: +86-0791-83969332



thermal catalysis reactions,<sup>11–14,20</sup> such as CO oxidation, in which high temperature and oxygen are always required.<sup>13,20</sup> In terms of thermodynamics, Cu<sub>2</sub>O can be easily oxidized under an oxidizing environment due to its very negative  $\Delta_r G_m^\ominus$  values (standard Gibbs free energy for reaction) even at room temperature (the value is calculated from the data of ref. 21 at 25 °C) from reaction (1). The endothermic feature of the reaction implies that the spontaneous change can be intensified when Cu<sub>2</sub>O is exposed to the real environment of the above-mentioned catalysis reactions. However, to the best of our knowledge, the transformations of Cu<sub>2</sub>O materials under these serious conditions and the derived influences have seldom been considered or systematically investigated.



In this study, a dramatic and sustainable enhancement in the activity on a catalytically used Cu<sub>2</sub>O nanoporous sphere sample for CO oxidation was discovered as compared to that on its fresh counterpart; the reason for this observation was investigated *via* a series of comprehensive characterizations among fresh and reused samples (the samples after one or more catalytic runs). It was observed that the surface of the Cu<sub>2</sub>O substrates would spontaneously transform into a multivalent composite interface with a certain and steady ratio of Cu(II) : Cu(I) after just one or more catalytic runs. The particularly higher composition of active chemisorbed oxygen on this reaction-induced or *in situ* restructured composite surface was determined and demonstrated to be the main contributor to speed up CO oxidation in a relatively low temperature range. These findings suggested that the real state derived from serious application conditions for Cu<sub>2</sub>O-containing materials should be noted, which could serve as clues to understand or design the functional surface structure for advanced applications of the Cu<sub>2</sub>O-based materials.

## 2. Experiments

### 2.1 Preparation of the Cu<sub>2</sub>O nanoporous sphere and reference samples

All chemicals were analytical grade reagents and used as received without further purification. Copper acetate monohydrate (Cu(CH<sub>3</sub>COO)<sub>2</sub> · H<sub>2</sub>O, AR, ~99.0%) was obtained from Aladdin. Diethylene glycol (DEG, GC, ≥ 99.0%) and D-(+)-glucose were obtained from Sigma-Aldrich. Polyvinylpyrrolidone (PVP, *M<sub>w</sub>*: ~55 000) was a product of Aldrich.

Briefly, 1.6 g PVP was dissolved in 25 mL DEG under magnetic stirring at 110 °C. Moreover, 0.60 g Cu(CH<sub>3</sub>COO)<sub>2</sub> · H<sub>2</sub>O and 1.3 g glucose were individually dissolved in 15 mL DEG, and then, the two solutions were simultaneously injected into the hot PVP solution; after about 2 h, the mixture turned yellow, suggesting the formation of the Cu<sub>2</sub>O particles. The mixture was cooled down to room temperature and centrifuged at 9000 rpm for 8 min to obtain the precipitate, which was washed with ethanol for at least four times and dried at 60 °C for 12 h in vacuum to obtain the Cu<sub>2</sub>O nanoporous sphere sample.

For reference, a Cu<sub>2</sub>O sample was calcined in a muffle furnace at 400 °C for 4 h to obtain the CuO sample. Other Cu<sub>2</sub>O nanomaterials with different morphologies such as cubic, octahedral, and 18-facet polyhedral particles were synthesized following the procedures described in ref. 22 and 23.

### 2.2 Characterization

X-ray diffraction (XRD) patterns of the samples were obtained using a Persee XD-3 X-ray diffractometer at a scan rate of 2° min<sup>-1</sup> in the angle (2θ) range from 10° to 90°. The wavelength of the incident radiation was 1.5406 Å (Cu Kα).

X-ray photoelectron spectroscopy (XPS) measurements were performed using an Axis Ultra DLD apparatus with monochromatized Al Kα (*hν* = 1486.6 eV) as the excitation source. XPS data were charge corrected using the adventitious carbon C 1s peak at 285.0 eV as a reference.

The morphology of the samples was characterized by transmission electron microscopy (TEM) using a JEOL JEM-2100 microscope operating at 200 kV. The samples were prepared by placing a drop of the ethanol suspension containing the sample powder on a carbon film-coated Cu grid (3 mm, 400 mesh), followed by drying under ambient conditions.

The scanning electron microscopy (SEM) measurements were performed using an FEI Quanta 200F microscope operating at 20.0 kV.

### 2.3 Chemical measurements

The catalytic performances of the samples for CO oxidation were measured *via* a continuous-flow fixed-bed quartz reactor using 60 mg sample. Prior to the test, the sample was purged with high purity Ar at 30 mL min<sup>-1</sup> for 20 min, and then, a reactant gas at the flow rate of 18 mL min<sup>-1</sup> was supplied into the reactor. The reactant gas flow was composed of 1 vol% CO and 1 vol% O<sub>2</sub> and balanced by N<sub>2</sub>. The reaction temperature was increased from room temperature at a step of 20 °C until 100% CO conversion was obtained. The reaction system was maintained at each temperature for 40 min to obtain experimental values at the steady state. The outlet gas was analyzed on-line using a GC-7890 gas chromatograph equipped with a thermal conductivity detector (TCD).

Temperature-programmed reduction by hydrogen (H<sub>2</sub>-TPR) and temperature-programmed desorption of carbon monoxide (CO-TPD) were performed on samples using a Micromeritics AutoChem II 2920 Chemisorption Analyzer. For the H<sub>2</sub>-TPR measurement, the degassed sample was exposed to a flow of 5.0 vol% hydrogen in Ar at the speed of 30 mL min<sup>-1</sup> and heated up to 400 °C at the rate of 10 °C min<sup>-1</sup> to obtain the TCD signal; the TCD apparatus was calibrated by quantitative reduction of a given quantity of CuO to metallic copper. For the TPD measurement, the degassed sample was exposed to 30 mL min<sup>-1</sup> Ar flow and heated up to 150 °C for 2 h; then, the system was cooled down to room temperature with Ar as the protector gas, and CO-contained flow was switched into the system for 1 h. After blowing Ar for 30 min, the sample was exposed to 30 mL min<sup>-1</sup> He flow and heated up to 600 °C at the rate of 10 °C min<sup>-1</sup> to obtain the TCD signals.



### 3. Results and discussion

The CO oxidation performance on the as-prepared (fresh) Cu<sub>2</sub>O particles was obtained as the change of CO conversion with temperature, as shown in Fig. 1A and denoted by the curve 1st. The reaction temperature window (RTW) on the sample was between 110 and 200 °C, which was close to the reported reaction temperature range for CO oxidation on Cu<sub>2</sub>O nanoparticles in the irregular shape.<sup>13,20</sup> One of the samples after the examination was not immediately removed from the reactor; after the temperature of the system naturally cooled down to room temperature by blowing pure N<sub>2</sub>, the examination procedure was repeated on the catalytically used sample. The corresponding curve was obtained and denoted as 2nd; interestingly, the RTW moved towards low temperature direction for about 60 °C in general, indicating a dramatic enhancement in the activity on the used sample for CO oxidation. To further understand the phenomenon, the examination procedures were repeated on the sample; the curves were obtained and denoted as 3rd to 9th. Among the 2nd to 9th curves, only small fluctuations of the RTW were observed, suggesting that the enhancement in CO conversion within this low RTW range was steady on the sample after just one catalytic run. The phenomenon was further disclosed by comparing the CO conversion at 80 °C and 140 °C (from the data of Fig. 1A) of the fresh sample and used samples obtained from different catalytic runs, as shown in Fig. 1B. It clearly exhibited a dramatic and sustainable enhancement in the activity on the used sample for CO oxidation after just one catalytic run as compared to that on its fresh counterpart. In addition, a reference CuO sample (obtained from the calcination procedure on fresh Cu<sub>2</sub>O) was also examined (seen in Fig. 1A); its performance was between that of the fresh Cu<sub>2</sub>O and used Cu<sub>2</sub>O samples. These results implied that the used Cu<sub>2</sub>O samples neither had a pure Cu<sub>2</sub>O nor a pure CuO structure.

To clarify the reason for the abovementioned observations, a series of characterizations was performed on fresh Cu<sub>2</sub>O, reference CuO, and typically used Cu<sub>2</sub>O samples, such as the sample obtained after the first catalytic run, *i.e.*, the sample directly derived from imposing one CO oxidation catalytic run on fresh Cu<sub>2</sub>O (denoted as Cu<sub>2</sub>O-1st CR), and the sample after the sixth catalytic run (denoted as Cu<sub>2</sub>O-6th CR). Fig. 2 shows the XRD patterns (A) and H<sub>2</sub>-TPR profiles (B) of the samples. In Fig. 2A, for fresh Cu<sub>2</sub>O (a) and reference CuO (d), the 2θ values of the diffraction peaks are in agreement with the standard diffraction angles of Cu<sub>2</sub>O (JCPDS cards no. 65-3288#) and those of CuO (JCPDS cards no. 65-2309#), indicating the well-developed and highly-ordered phase structure of both samples. For the Cu<sub>2</sub>O-1st CR and Cu<sub>2</sub>O-6th CR samples (b and c), although two small and weak diffractions located at around 2θ of 38.8° and 66.2° suggested the existence of CuO structure, the main diffractions were closer to those of fresh Cu<sub>2</sub>O, indicating that the main phase or body of the two samples undergoing the catalytic runs was retained as Cu<sub>2</sub>O crystalline. The abovementioned phase differences among samples also led to their different redox properties; as shown in Fig. 2B, the H<sub>2</sub>-consumption peaks of the two used Cu<sub>2</sub>O samples nearly overlapped, and the area was higher than that of fresh Cu<sub>2</sub>O, but lower than that of CuO, suggesting that there were additional species to exhaust H<sub>2</sub> on used samples as compared to those on fresh Cu<sub>2</sub>O. In addition, the lower temperature for the H<sub>2</sub>-consumption peak for Cu<sub>2</sub>O-1st CR and Cu<sub>2</sub>O-6th CR samples (205 °C) as compared to that for the fresh substrate (250 °C) was observed, suggesting that the redox ability of Cu<sub>2</sub>O was obviously improved after just one catalytic run, which could have caused the enhanced activity observed on the used samples.

Fig. 3 shows the images of four samples obtained from the TEM measurements. The fresh Cu<sub>2</sub>O sample (Fig. 3a) is shown as the nanoporous sphere within the size range of 250–400 nm. Cu<sub>2</sub>O-1st CR (Fig. 3b), Cu<sub>2</sub>O-6th CR (Fig. 3c), and CuO (Fig. 3d)

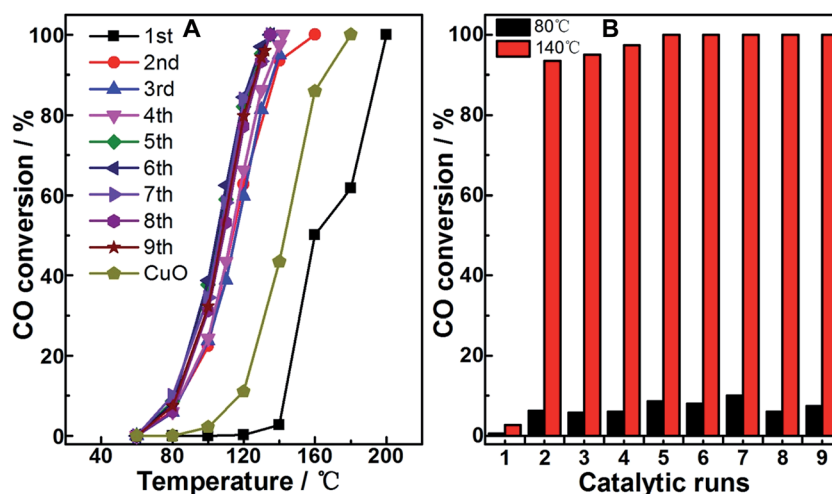


Fig. 1 (A) CO conversion as the function of reaction temperature on the as-prepared (fresh) Cu<sub>2</sub>O (1st), the corresponding repeatedly used samples (from 2nd to 9th), and CuO sample (obtained from calcination at 400 °C for 4 h). (B) Comparison of the conversion at 80 °C and 140 °C among the fresh and used Cu<sub>2</sub>O samples.



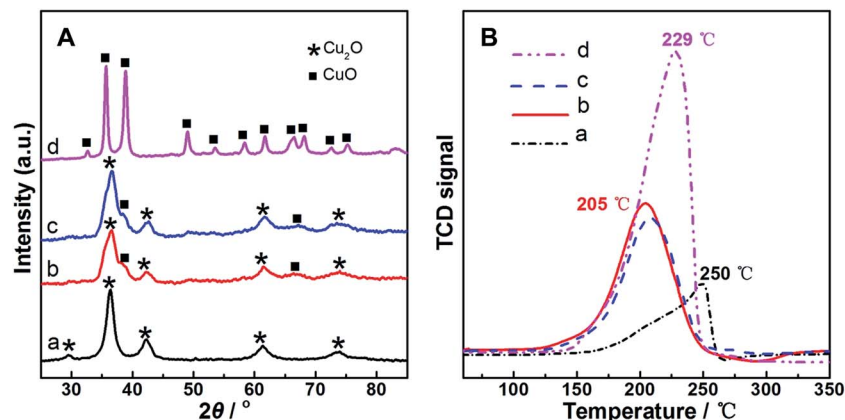


Fig. 2 XRD patterns (A) and  $\text{H}_2$ -TPR profiles (B) on representative samples. (a) Fresh  $\text{Cu}_2\text{O}$ ; (b)  $\text{Cu}_2\text{O}$ -1st CR (used  $\text{Cu}_2\text{O}$  after one catalytic run); (c)  $\text{Cu}_2\text{O}$ -6th CR (used  $\text{Cu}_2\text{O}$  after six catalytic runs); and (d)  $\text{CuO}$ .

appeared similar to  $\text{Cu}_2\text{O}$  substrate; this suggested the insignificant changes in shape among the samples. However, from the detailed local features shown in the HRTEM images of the samples,  $d$ -spacing values measured at 0.302 nm and 0.246 nm for the fresh  $\text{Cu}_2\text{O}$  sample were close to the standard values of  $\text{Cu}_2\text{O}$ -[110] and  $\text{Cu}_2\text{O}$ -[111] planes (JCPDS cards no. 65-3288). Only the  $d$ -spacing value around 0.252 nm pertinent to the  $\text{CuO}$ -[002] plane (JCPDS cards no. 65-2309) was observed in the  $\text{CuO}$  sample, confirming the pure  $\text{CuO}$  crystalline feature of the sample, consistent with the XRD observation. In contrast, both  $\text{Cu}_2\text{O}$ -[110], -[200] ( $d$ -spacing value at 0.211 nm) and  $\text{CuO}$ -[002], -[111] ( $d$ -spacing value at 0.231 nm) planes could be resolved on  $\text{Cu}_2\text{O}$ -1st CR and  $\text{Cu}_2\text{O}$ -6th CR samples; this indicated the co-existence of the  $\text{Cu}_2\text{O}$  and  $\text{CuO}$  structures, *i.e.*, the  $\text{Cu(I)}\text{-Cu(II)}$  multivalent oxide composite interface derived from  $\text{Cu}_2\text{O}$  during the CO oxidation reaction, in both the used  $\text{Cu}_2\text{O}$  samples.

XPS measurements were employed to quantify the surface composition of the samples, and the spectra are shown in Fig. 4. For our  $\text{Cu}_2\text{O}$  sample (Fig. 4A(a)), two peaks located at 932.2 eV and 951.9 eV were close to the reported Cu  $2p_{3/2}$  and Cu  $2p_{1/2}$  spectra of the common  $\text{Cu}_2\text{O}$  particles.<sup>24,25</sup> In contrast, other samples produced two main peaks at the higher binding energy range around 934.0 eV and 954.1 eV, which were close to the standard Cu  $2p_{3/2}$  and Cu  $2p_{1/2}$  spectra of  $\text{CuO}$ , respectively. Furthermore, the shakeup satellite peaks within 939.6 and 945.8 eV and around 962.7 eV were also the features of  $\text{CuO}$ , being different from those of  $\text{Cu}_2\text{O}$ ;<sup>26,27</sup> these features indicated that  $\text{CuO}$  was the main component on the surfaces of  $\text{Cu}_2\text{O}$ -1st CR,  $\text{Cu}_2\text{O}$ -6th CR, and  $\text{CuO}$  samples (Fig. 4A(b–d), respectively). In addition, it should be noted that the Cu 2p spectra for  $\text{Cu}_2\text{O}$ -1st CR and  $\text{Cu}_2\text{O}$ -6th CR samples displayed broader shoulder peaks in comparison with the relatively symmetrical peaks for the  $\text{CuO}$  sample. Moreover, the co-existence of  $\text{Cu}_2\text{O}$  and  $\text{CuO}$  in  $\text{Cu}_2\text{O}$ -1st CR and  $\text{Cu}_2\text{O}$ -6th CR samples was confirmed *via* the HRTEM measurements. Hence, careful peak-fitting measurements focused on Cu 2p peaks of  $\text{Cu}_2\text{O}$  and  $\text{CuO}$  for the two samples were performed, as shown in Fig. 4A(b and c). Interestingly, these two samples showed close ratios of  $\text{Cu(II)} : \text{Cu(I)}$ ,

which were all around 4.0, suggesting that a stable  $\text{Cu(I)}\text{-Cu(II)}$  multivalent oxide composite surface with almost unchanged  $\text{Cu(II)} : \text{Cu(I)}$  ratio was derived from the fresh  $\text{Cu}_2\text{O}$  surface through just one catalytic run of CO oxidation. Besides Cu 2p spectra, O 1s spectra were also resolved for the samples, as shown in Fig. 4B. In general, two distinguished peaks within the 526.0–538 eV range were observed for all the samples, which could be assigned to lattice oxygen  $\text{O}_\text{L}$  and chemisorbed oxygen  $\text{O}_\text{CA}$  (at higher binding energy).<sup>28,29</sup> The ratios of  $\text{O}_\text{CA} : \text{O}_\text{L}$  in  $\text{Cu}_2\text{O}$ ,  $\text{Cu}_2\text{O}$ -1st CR,  $\text{Cu}_2\text{O}$ -6th CR, and  $\text{CuO}$  were estimated to be 0.46, 5.3, 5.7, and 1.9, respectively; moreover,  $\text{Cu}_2\text{O}$ -1st CR and  $\text{Cu}_2\text{O}$ -6th CR showed similar  $\text{O}_\text{CA} : \text{O}_\text{L}$  ratio (averaged at 5.5) on their surfaces, further confirming the stable surface composition of this reaction-induced or *in situ* restructured sample from the  $\text{Cu}_2\text{O}$  substrate. Notably,  $\text{O}_\text{CA}$  was generally believed to be the key active oxygen species for the oxidation reactions;<sup>28,29</sup> however, the highest ratios between the surface oxygen and lattice oxygen were always found to be not more than or just around 2.0 among most of the reported  $\text{Cu}_x\text{O}$ -based catalysts such as  $\text{Cu}_2\text{O}$ -,  $\text{CuO}$ -based, or  $\text{Cu(I)}\text{-Cu(II)}$  composite oxide catalysts.<sup>28–30</sup> In total contrast, a particularly high  $\text{O}_\text{CA}$  surface composition with the  $\text{O}_\text{CA} : \text{O}_\text{L}$  ratio around 5.5 was observed in our  $\text{Cu}_2\text{O}$ -1st CR and  $\text{Cu}_2\text{O}$ -6th CR samples, which could be an important factor to facilitate CO oxidation. Considering that oxygen content was excessive in our catalytic measurements, based on a referee's advice, a reference sample obtained by heating fresh  $\text{Cu}_2\text{O}$  to 200 °C in air for 2 h was also measured by XPS to investigate the influence of this atmosphere; the spectra of the sample are labeled as (e)  $\text{Cu}_2\text{O}$ -A200 in Fig. 4. The general feature of the sample was similar to that of the  $\text{CuO}$  sample, except for the distinguished  $\text{Cu(II)} : \text{Cu(I)}$  ratio at 6.0 and  $\text{O}_\text{CA} : \text{O}_\text{L}$  ratio of 2.2. Although better CO oxidation activity with a lowered reaction temperature range of 80–180 °C as compared to that on the  $\text{Cu}_2\text{O}$  sample was observed in the sample (not shown), due to different surface compositions, the sample was still less active in comparison with  $\text{Cu}_2\text{O}$ -1st CR and  $\text{Cu}_2\text{O}$ -6th CR samples, which were restructured during CO oxidation. The result suggested that the atmosphere played an important role in restructuring the surface composition of the  $\text{Cu}_2\text{O}$





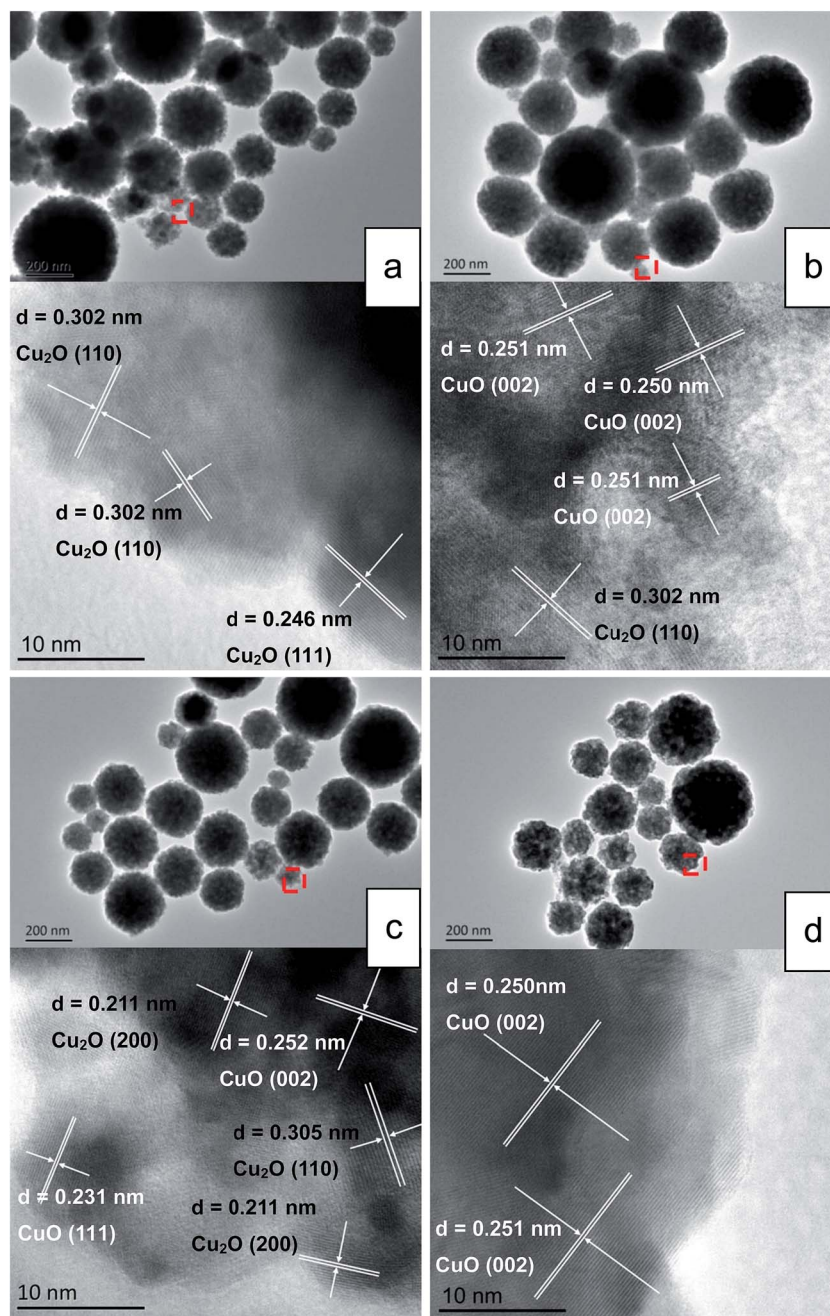


Fig. 3 General appearance and local details of morphology for the representative samples. (a) Fresh  $\text{Cu}_2\text{O}$ ; (b)  $\text{Cu}_2\text{O}$ -1st CR; (c)  $\text{Cu}_2\text{O}$ -6th CR; and (d)  $\text{CuO}$  (up: TEM images; down: HRTEM images).

substrate. However, the deliberately imposed conditions to process the sample need more careful investigation for further improving the performance. Based on the abovementioned characterizations, it can be recognized that due to the surface restructuring effect of fresh  $\text{Cu}_2\text{O}$  present in the first catalytic run of CO oxidation, the pure  $\text{Cu}_2\text{O}$  surface would *in situ* and spontaneously transform into distinguished Cu-oxides composite interface with certain and steady surface distributions of oxidative Cu and active oxygen species.

For CO catalytic oxidation, the interaction between CO and catalyst surface was believed to be a key factor influencing the

reaction behavior and activity. As an attempt to illustrate this interaction in our samples, herein, CO-TPD measurements were employed, as shown in Fig. 5. In comparison with those of the  $\text{Cu}_2\text{O}$  and  $\text{CuO}$  samples, the desorption peaks of the two used  $\text{Cu}_2\text{O}$  moved towards lower temperature range, indicating superior low-temperature activation effect on the multivalent composite surface of the two used  $\text{Cu}_2\text{O}$  samples as compared to that of the unitary  $\text{Cu}_2\text{O}$  or  $\text{CuO}$  surface. Notably, the desorption peaks for the two used  $\text{Cu}_2\text{O}$  samples almost overlapped, and the observation was similar to previous characterizations, which further confirmed that even through just one catalytic run, not



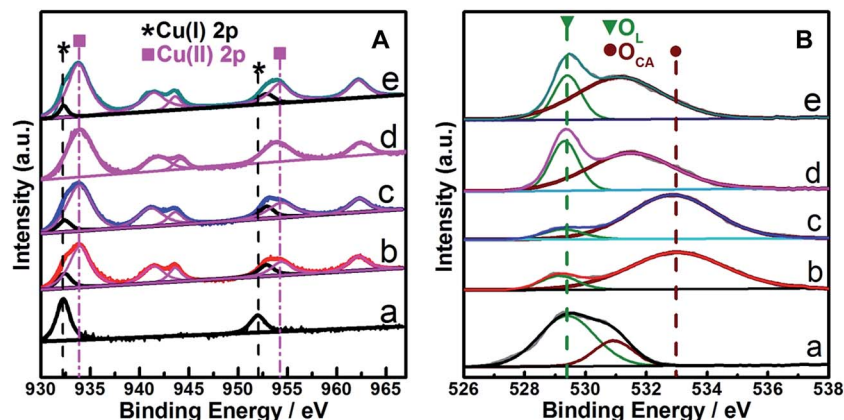


Fig. 4 Cu 2p (A) and O 1s (B) XPS spectrum of representative samples. (a) Fresh  $\text{Cu}_2\text{O}$ ; (b)  $\text{Cu}_2\text{O}$ -1st CR; (c)  $\text{Cu}_2\text{O}$ -6th CR; (d)  $\text{CuO}$ ; and (e)  $\text{Cu}_2\text{O}$ -A200 (obtained by heating  $\text{Cu}_2\text{O}$  in air to 200 °C for 2 h).

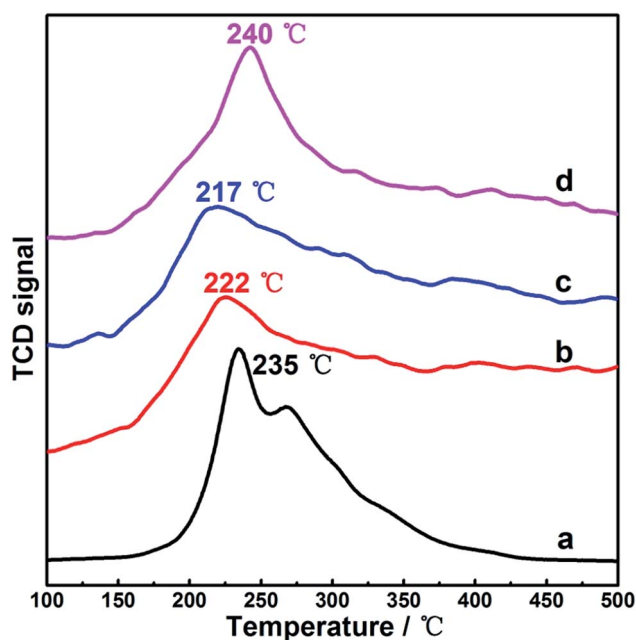


Fig. 5 CO-TPD profiles on representative samples. (a) Fresh  $\text{Cu}_2\text{O}$ ; (b)  $\text{Cu}_2\text{O}$ -1st CR; (c)  $\text{Cu}_2\text{O}$ -6th CR; and (d)  $\text{CuO}$ .

only a stable composite surface but also steady chemical properties could be achieved on the  $\text{Cu}_2\text{O}$  substrate. Djurišić *et al.*<sup>29</sup> also carefully inspected the surface change between the as-prepared and used states on a hydrothermally synthesized  $\text{Cu}_x\text{O}$  sample for CO oxidation. They found that the surface of their sample was not stable since a continuous decrease in the ratio of lattice oxygen to surface oxygen with the increasing catalytic cycling was observed. This observation suggested that although multivalent  $\text{Cu}_x\text{O}$  interface had been demonstrated to be catalytically more competitive than pure  $\text{Cu}_2\text{O}$  and  $\text{CuO}$  surfaces, obtaining a stable surface with desirable properties could still require extensive study and attention. Relatively, present findings suggested that employment of a reactive redox atmosphere and certain thermal conditions to process  $\text{Cu}_2\text{O}$ , such as CO oxidation on our sample, could be a convenient way

to acquire  $\text{Cu}_2\text{O}$ -based materials with finely modulated and stable surfaces. In addition, the outlet gas from CO-TPD was analyzed *via* mass spectrometry; in contrast to the mixture of CO and  $\text{CO}_2$  desorbed from the pure  $\text{Cu}_2\text{O}$  surface, the desorption from  $\text{Cu}_2\text{O}$ -1st CR and  $\text{Cu}_2\text{O}$ -6th CR samples was almost fully composed by  $\text{CO}_2$ ; this indicated that the introduced CO could be more easily and fully converted to  $\text{CO}_2$  on our surface-restructured  $\text{Cu}_2\text{O}$  samples. The phenomenon was directly connected to the particularly higher surface compositions of active chemisorbed oxygen as compared to that of the pure  $\text{Cu}_2\text{O}$  sample (disclosed by previous XPS measurements) since there was no other O-source in the environment of the CO-TPD measurements. Therefore, it was reasonable to believe that the most attractive advantage of our surface-restructured  $\text{Cu}_2\text{O}$  sample could be its high efficiency in producing large amounts of the active chemisorbed oxygen during CO oxidation, which was the main impetus to speed up CO conversion to  $\text{CO}_2$  in low temperature range.

As is known, many studies on  $\text{Cu}_2\text{O}$ -based materials for catalysis applications have been focused on the influence of different physical features of samples;<sup>13,14,19</sup> for example, Huang *et al.*<sup>14</sup> showed the detailed impact of crystalline surface on the CO oxidation behavior by employing  $\text{Cu}_2\text{O}$  nanocrystals in different shapes. We also extended similar catalytic measurements on other  $\text{Cu}_2\text{O}$  nanosubstrates with different morphologies such as cubic (C- $\text{Cu}_2\text{O}$ ), octahedral (O- $\text{Cu}_2\text{O}$ ), and 18-facet polyhedral (P- $\text{Cu}_2\text{O}$ ) nanoparticles. Fig. 6 shows the morphology and corresponding CO conversion curves of these samples. The SEM images show the well-constructed shape of the samples, and the corresponding CO oxidation measurements on the fresh sample, the used sample after one catalytic run, and the used sample after six catalytic runs were conducted. Irrespective of the initial state and shape of the  $\text{Cu}_2\text{O}$  nanoparticles, the dramatic and sustainable enhancement in the activity on the used samples as compared to that on their fresh counterparts were repeatedly observed, similar to the observations on nanoporous sphere sample. Hence, these observations suggested that the reaction-induced or *in situ* restructuring effect under the presence of redox atmosphere discovered in this study might be a common feature of the  $\text{Cu}_2\text{O}$  substrates, which



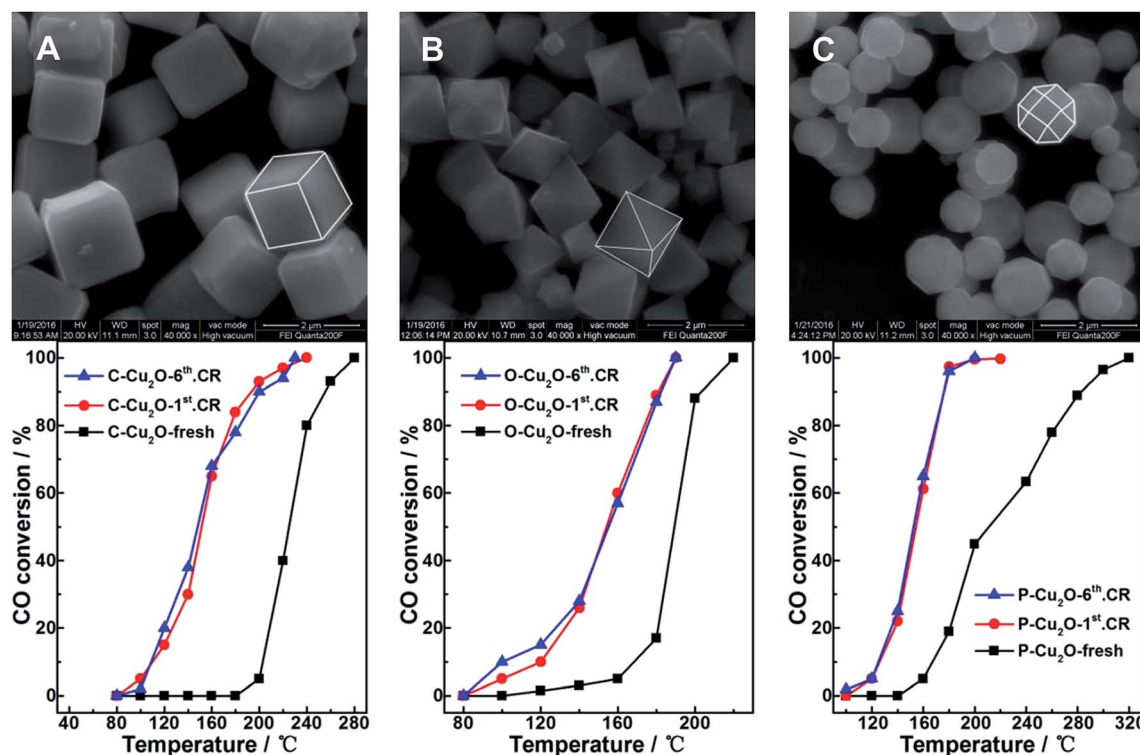


Fig. 6 SEM morphologies of the Cu<sub>2</sub>O nanomaterials in different shapes and corresponding dependence of CO conversion on reaction temperature among fresh sample and used samples (after one and six catalytic runs). (A) Cubic particles (C-Cu<sub>2</sub>O); (B) octahedral particles (O-Cu<sub>2</sub>O); and (C) 18-facet polyhedral particles (P-Cu<sub>2</sub>O).

could lead to notable changes in both the surface structure and corresponding performance of the Cu<sub>2</sub>O-containing samples.

## 4. Conclusions

Irrespective of the initial states and shapes, the pure Cu(I) surface of the fresh Cu<sub>2</sub>O nanomaterials would spontaneously transform *in situ* into a multivalent and stable Cu(I)-Cu(II) composite surface (with almost unchanged Cu(II) : Cu(I) and O<sub>CA</sub> : O<sub>L</sub> ratios) through just one catalytic run of CO oxidation. The higher surface composition of active chemisorbed oxygen and the corresponding more effective interaction with CO contributed to the dramatic activity enhancement on the used samples as compared to that on the fresh Cu<sub>2</sub>O substrates. These observations suggest that this *in situ* restructuring effect of the Cu<sub>2</sub>O component should be noted as a common feature of the Cu<sub>2</sub>O-based materials, especially when serious application conditions such as redox atmosphere and certain thermal conditions are employed; these findings can be referenced as clues not only for understanding the real state of the Cu<sub>2</sub>O-containing samples in applications, but also for manipulating the surface structure of Cu<sub>2</sub>O-based materials for advanced applications through convenient atmosphere-controlled measurements.

## Acknowledgements

Authors gratefully acknowledge the financial support provided by the National Natural Science Foundation of China (NSFC,

No. 21003071 and No. 21563018) and Doctoral Fund of Ministry of Education of China (No. 20093601120007).

## References

- 1 C. H. Kuo and M. H. Huang, *Nano Today*, 2010, **5**, 106–116.
- 2 P. Lignier, R. Bellabarba and R. P. Tooze, *Chem. Soc. Rev.*, 2012, **41**, 1708–1720.
- 3 J. Zhang, J. Liu, Q. Peng, X. Wang and Y. Li, *Chem. Mater.*, 2006, **18**, 867–871.
- 4 L. Zhang, Z. Cui, Q. Wu, D. Guo, Y. Xu and L. Guo, *CrystEngComm*, 2013, **15**, 7462–7467.
- 5 H. Bao, Z. Zhang, Q. Hua and X. W. Huang, *Langmuir*, 2014, **30**, 6427–6436.
- 6 Z. Wang, R. Li and Q. Chen, *ChemPhysChem*, 2015, **16**, 2415–2423.
- 7 J. Chen, S. Shen, P. Guo, M. Wang, P. Wu, X. Wang and L. J. Guo, *Appl. Catal., B*, 2014, **152–153**, 335–341.
- 8 R. M. Mohamed and E. S. Aazam, *Appl. Catal., A*, 2014, **480**, 100–107.
- 9 L. Wu, L. K. Tsui, N. Swami and G. Zangari, *J. Phys. Chem. C*, 2010, **114**, 11551–11556.
- 10 R. Ji, W. Sun and Y. Chu, *ChemPhysChem*, 2013, **14**, 3971–3976.
- 11 Y. P. Zhang, Y. C. Jiao, Y. S. Yang and C. L. Li, *Tetrahedron Lett.*, 2013, **54**, 6494–6497.
- 12 N. Chatterjee, R. Pal, S. Sarkar and A. K. Sen, *Tetrahedron Lett.*, 2015, **56**, 3886–3889.



- 13 M. Leng, M. Liu, Y. Zhang, Z. Wang, C. Yu, X. Yang, H. Zhang and C. Wang, *J. Am. Chem. Soc.*, 2010, **132**, 17084–17087.
- 14 Q. Hua, T. Cao, H. Bao, Z. Jiang and X. W. Huang, *ChemSusChem*, 2013, **6**, 1966–1972.
- 15 J. Shi, J. Li, X. Huang and Y. Tan, *Nano Res.*, 2011, **4**, 448–459.
- 16 W. C. Huang, L. M. Lu, Y. C. Yang and M. H. Huang, *J. Am. Chem. Soc.*, 2012, **134**, 1261–1267.
- 17 B. D. Yu and P. Yang, *J. Am. Chem. Soc.*, 2009, **131**, 3756–3761.
- 18 J. Wang, G. Ji, Y. Liu, M. A. Gondal and X. Chang, *Catal. Commun.*, 2014, **46**, 17–21.
- 19 S. Sun, *Nanoscale*, 2015, **7**, 10850–10882.
- 20 S. Y. Zhang, H. Liu, C. C. Sun, P. F. Liu, L. C. Li, Z. H. Yang, X. Feng, F. W. Huo and X. H. Lu, *J. Mater. Chem. A*, 2015, **3**, 5294–5298.
- 21 D. R. Lide, Standard Thermodynamic Properties of Chemical Substances, in *CRC Handbook of Chemistry and Physics*, *P<sub>788</sub>-P<sub>804</sub>*, CRC, Boca Raton, Florida, 90th edn, 2009.
- 22 L. Gou and C. J. Murphy, *Nano Lett.*, 2003, **3**, 231–234.
- 23 C. Lu, L. Qi, J. Yang, X. Wang, D. Zhang, J. Xie and J. Ma, *Adv. Mater.*, 2005, **17**, 2562–2567.
- 24 C. K. Wu, M. Yin, S. O. Brien and J. T. Koberstein, *Chem. Mater.*, 2006, **18**, 6054–6058.
- 25 C. C. Chusuei, M. A. Brookshier and D. W. Goodman, *Langmuir*, 1999, **15**, 2806–2808.
- 26 K. Zhong, J. Xue, Y. Mao, C. Wang, T. Zhai, P. Liu, X. Xia, H. Li and Y. Tong, *RSC Adv.*, 2012, **2**, 11520–11528.
- 27 M. S. P. Francisco and V. R. Mastelaro, *J. Phys. Chem. B*, 2001, **105**, 10515–10522.
- 28 D. A. Svintsitskiy, A. P. Chupakhin, E. M. Slavinskaya, O. A. Stonkus, A. I. Stadnichenko, S. V. Koscheev and A. I. Boronin, *J. Mol. Catal. A: Chem.*, 2013, **368–369**, 95–106.
- 29 M. Y. Guo, F. Liu, J. Tsui, A. A. Voskanyan, A. M. C. Ng, A. B. Djurišić, W. K. Chan, K. Y. Chan, C. Liao, K. Shih and C. Surya, *J. Mater. Chem. A*, 2015, **3**, 3627–3632.
- 30 Y. L. Zheng, D. S. Mao, S. S. Sun and G. Y. Fu, *J. Nanopart. Res.*, 2015, **17**, 471.

